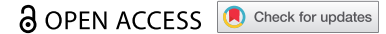



RESEARCH PAPER



Mice deficient in UXT exhibit retinitis pigmentosa-like features via aberrant autophagy activation

Mingyu Pan^a, Yue Yin^a, Xinxia Wang^a, Quanyi Wang^a, Lele Zhang ^b, Haiyang Hu ^a, and Chen Wang^a

^aState Key Laboratory of Natural Medicines, School of Life Science and Technology, China Pharmaceutical University, Nanjing, China; ^bState Key Laboratory of Cell Biology, CAS Center for Excellence in Molecular Cell Science, Shanghai Institute of Biochemistry and Cell Biology, Chinese Academy of Sciences, University of Chinese Academy of Sciences, Shanghai, China

ABSTRACT

UXT (ubiquitously expressed prefoldin like chaperone), a small chaperone-like protein, is widely expressed in diverse human and mouse tissues and is more abundant in retina and kidney. However, the functional characterization of UXT at tissue level was largely unknown. Here, we reported that mice deficient in UXT exhibited salient features of retinal degenerative disease, similar to retinitis pigmentosa. Conditional knockout (CKO) of *Uxt* led to retinal degeneration and pigmentation in mice retina along with significant alterations of retinitis pigmentosa-related genes, which indicated UXT might be associated with retinal degenerative disease sharing key features to retinitis pigmentosa. Consistently, the electroretinogram (ERG) responses were dramatically impaired in *uxt* CKO retinas. Strong degenerative features were observed in *uxt* CKO retinas, including specific and progressive reduction of photoreceptor cells and increased numbers of apoptotic cells. Intriguingly, macroautophagic/autophagic flux was enhanced in *uxt* CKO retina. Mechanistically, we found UXT was indispensable to suppress photoreceptor apoptotic cell death by inhibiting autophagy through regulating the activity of MTOR (mechanistic target of rapamycin kinase), a key negative regulator of autophagy. Conversely, knockdown of UXT induced the robust expression of the canonical autophagy-related genes and boosted autophagic flux and apoptosis, finally resulting in severe retina degeneration in *uxt* CKO mice. Taken together, our study reveals a vital role of UXT in preventing retina from degeneration. The loss of UXT results in a hyper-autophagic state leading to massive retinal degeneration. Therefore, UXT may be a crucial target for retinal degenerative disease.

Abbreviations: 3-ma: 3-methyladenine; casp3: caspase 3; cko: conditional knockout; erg: electroretinogram; gapdh: glyceraldehyde-3-phosphate dehydrogenase; map1lc3b/lc3b: microtubule-associated protein 1 light chain 3; mtor: mechanistic target of rapamycin kinase; parp: poly (adp-ribose) polymerase family; rna-seq: rna sequencing; rp: retinitis pigmentosa; rps6kb1/s6k: ribosomal protein s6 kinase b1; sqstm1: sequestosome 1; tunel: terminal deoxynucleotidyl transferase mediated dntp nick-end labeling; *uxt*: ubiquitously expressed prefoldin like chaperone.

ARTICLE HISTORY

Received 30 April 2020
Revised 29 June 2020
Accepted 9 July 2020

KEYWORDS

Apoptosis; autophagy; degeneration; MTOR; photoreceptor; retinitis pigmentosa; UXT


Introduction

The retina is a thin sheet of neural tissue in the eye, which senses light and transmits relevant information to the brain via the optic nerve. The vertebrate retina consists of six types of neurons and one type of glial cells (Müller glial cells), which form three cellular layers: photoreceptors in the outer nuclear layer (ONL), horizontal, bipolar, and amacrine interneurons and Müller glial cells in the inner nuclear layer (INL), and ganglion and displaced amacrine cells in the ganglion cell layer (GCL). The detection of light stimuli is mediated by photoreceptors, which contain two basic subtypes: rods and cones. The rod and cone photoreceptors are responsible for night and daylight vision, respectively. Typically, mouse retinal genesis begins as early as embryonic day 11 (E11), and retinal maturation is complete at postnatal day 30 (P30) [1].

Retinitis pigmentosa (RP) is a hereditary retinopathy that affects approximately 2.5 million people worldwide and shows a prevalence ranging from 1/3500 to 1/5000 among different populations [2,3]. It is characterized by progressive loss of rods and cones and causes severe visual dysfunction and eventual blindness in bilateral eyes [3]. RP exhibits great genetic heterogeneity with 83 disease causative genes involved in its etiology, among which 58 are implicated in the autosomal recessive form. Most of such cases are due to mutations in a single gene, representing a significant cause of blindness. These mutations occur mainly in the photoreceptor cells (rods and cones) and, to a much lesser extent, in the retinal pigment epithelium (RPE) cells [4].

Although several causative mutations of RP have been identified, the mechanisms underlying the death of photoreceptors are still unclear, therefore currently, no treatment is available [5]. It is very important to know the physiology and

CONTACT Haiyang Hu  haiyanghu@cpu.edu.cn; Chen Wang  cwang1971@cpu.edu.cn  State Key Laboratory of Natural Medicines, School of Life Science and Technology, China Pharmaceutical University, Nanjing 211198, China

 Supplemental data for this article can be accessed [here](#).

© 2020 The Author(s). Published by Informa UK Limited, trading as Taylor & Francis Group.

This is an Open Access article distributed under the terms of the Creative Commons Attribution-NonCommercial-NoDerivatives License (<http://creativecommons.org/licenses/by-nc-nd/4.0/>), which permits non-commercial re-use, distribution, and reproduction in any medium, provided the original work is properly cited, and is not altered, transformed, or built upon in any way.

the possible alterations of the RP retina. Currently, autophagy and the dysregulation caused by different sources of oxidative stress are associated with and contributed to RP retinal changes [6]. Autophagy was first described in retina forty years ago [7]. Components of the autophagy pathway have been found in retina and important autophagy-related proteins have been detected in different retinal layers. Autophagy has been shown to initiate apoptosis and contribute to photoreceptor death [8]. The MTOR pathway is essential for suppressing autophagy [9]. Furthermore, many genes related to MTOR signaling pathway are decreased in numerous experimental RP models [10]. These observations indicate that MTOR pathway might be of importance in regulating autophagy in retina, loss of which may associate with pathological alterations in RP retina. Consistently, activation of MTORC1 by loss of its negative regulator TSC1 is sufficient to promote survival of starving cones of rd1 mouse [11].

In this study, we discovered a novel MTOR regulator, UXT (ubiquitously expressed prefoldin like chaperone), which is indispensable for normal retina function through promoting MTOR activity. UXT is a small chaperone-like protein, which has been shown to be involved in modulating innate immunity, inflammation [12–14] and angiogenesis in zebrafish development [15]. Although UXT is widely expressed in most human and mouse tissues [16], its functional significance was less characterized and largely unknown. Through integrating morphology and histological experiments, retinal function assays and underlying dynamic transcriptome changes in retinas of *uxt* CKO mice, we found mice deficient in UXT exhibited key features similar to retinitis pigmentosa. Electroretinogram responses were dramatically impaired in *uxt* CKO mice, which was accompanied by degenerative features including progressively reduced numbers of photoreceptor cells and increased numbers of apoptotic cells. Notably, *uxt* CKO retina displayed enhanced autophagic flux. Mechanistically, UXT interacted with MTOR and repressed autophagy by boosting MTOR activity.

Results

UXT is associated with retinitis pigmentosa

To explore the function of UXT at tissue level, we took advantage of the public RNA-seq data of mouse tissues and found that UXT was abundantly expressed in adult retina (Figure 1A). Using real-time PCR, we confirmed this result and observed the generally higher expression of *Uxt* mRNA in early stages of mice retina development (Figure 1B), suggesting UXT may play a role during retinogenesis. In addition, we found UXT was markedly expressed in photoreceptor segment of retina by immunofluorescence (Fig. S1A). In line with this, we detected similar expression pattern between UXT and well-known photoreceptor cell markers (e.g., RHO [rhodopsin] and OPN1SW) based on public single-cell RNA-seq data of mouse retina (Fig. S1B and S1C). To further investigate the role of UXT in retina, *uxt* flox mice were constructed. To delete *Uxt* specifically in the developing retina, we crossed the *uxt* flox line with the *Vsx2/Chx10-Cre* transgenic mice to obtain *uxt* conditional knockout (*uxt*

CKO) mice. To examine the efficiency of *Uxt* deletion, we analyzed UXT expression by western blot and immunofluorescence on *Uxt*^{flox/flox} and *uxt*^{flox/flox}; *Vsx2-Cre* retinas at P1 (postnatal day 1). We observed essentially no signal of UXT in *uxt*^{flox/flox}; *Vsx2-Cre* retinas at P1 (Figure 1C and D), demonstrating that *Uxt* was efficiently deleted in the developing retina at an early stage. We then carried out RNA-seq experiment to measure molecular changes at gene expression level in *uxt* CKO retinas. Conditional knockout of *Uxt* led to dramatic gene expression changes in mouse retina at P30, as reflected by only moderately correlated expression between *uxt* CKO and control retinas (correlation: 0.61 ~ 0.74). By contrast, gene expression was perfectly correlated between biological replicates for both *uxt* CKO retinas and control retinas (correlation: 0.96 ~ 0.99) (Figure 1E and S1D). Consistently, the principal component analysis (PCA) result also demonstrated that more than 70% of total gene expression variance was explained by the factor of *uxt* CKO (Fig. S1E). In total, we identified 2,211 differentially expressed (DE) genes with at least two-fold changes in *uxt* CKO retina, including 1,290 up- and 921 downregulated genes (Figure 1F, FDR<0.01, absolute LFC>1, Table S1). Intriguingly, the downregulated DE genes were strongly enriched in the biological processes such as visual perception, photoreceptor cell maintenance, phototransduction and eye photoreceptor cell development (Figure 1G and Table S2, FDR<0.001, fold-enrichment > 8), all of which were directly related to retinal-related biological process required for normal retina function. In addition, cellular components analysis demonstrated that the downregulated DE genes were strongly enriched in photoreceptor segments (Figure 1H and Table S2, FDR<0.001, fold-enrichment>9), where UXT was also preferentially localized as demonstrated by immunofluorescence experiment (Fig. S1A). These results suggest that UXT may involve in preserving normal retina function by orchestrating genes required for visual perception and phototransduction within photoreceptor cells. Loss of key genes required for retina photoreceptor functionality usually leads to retinal defects [17]. Notably, we found a strong link between the downregulated DE genes and retinal diseases, especially for the association with retinitis pigmentosa (Figure 1I and Table S3, FDR<0.001, fold-enrichment>8). In line with this result, manually curated canonical genes of retinitis pigmentosa were mostly decreased in *uxt* CKO retina (Figure 1J and Table S3, Wilcoxon rank sum test, p-value<0.001). To further confirm this result, we performed fundus photograph to examine retinopathy in control and *uxt* CKO mice. Compared with control mice, retinal degeneration and pigmentation appeared in 1-month-old *uxt* CKO mice (Figure 1K). The retinopathy was apparently more severe in 3-month-old *uxt* CKO mice (Figure 1L). Therefore, severe defects seemed to occur progressively in *uxt* CKO retina, which is similar to the symptom of retinitis pigmentosa.

*Impaired ERG responses in the *uxt* CKO mice*

To examine whether *uxt* CKO disrupted retinal function *in vivo*, full-field electroretinogram (ERG) recordings were performed to measure retinal function in *uxt* CKO mice at

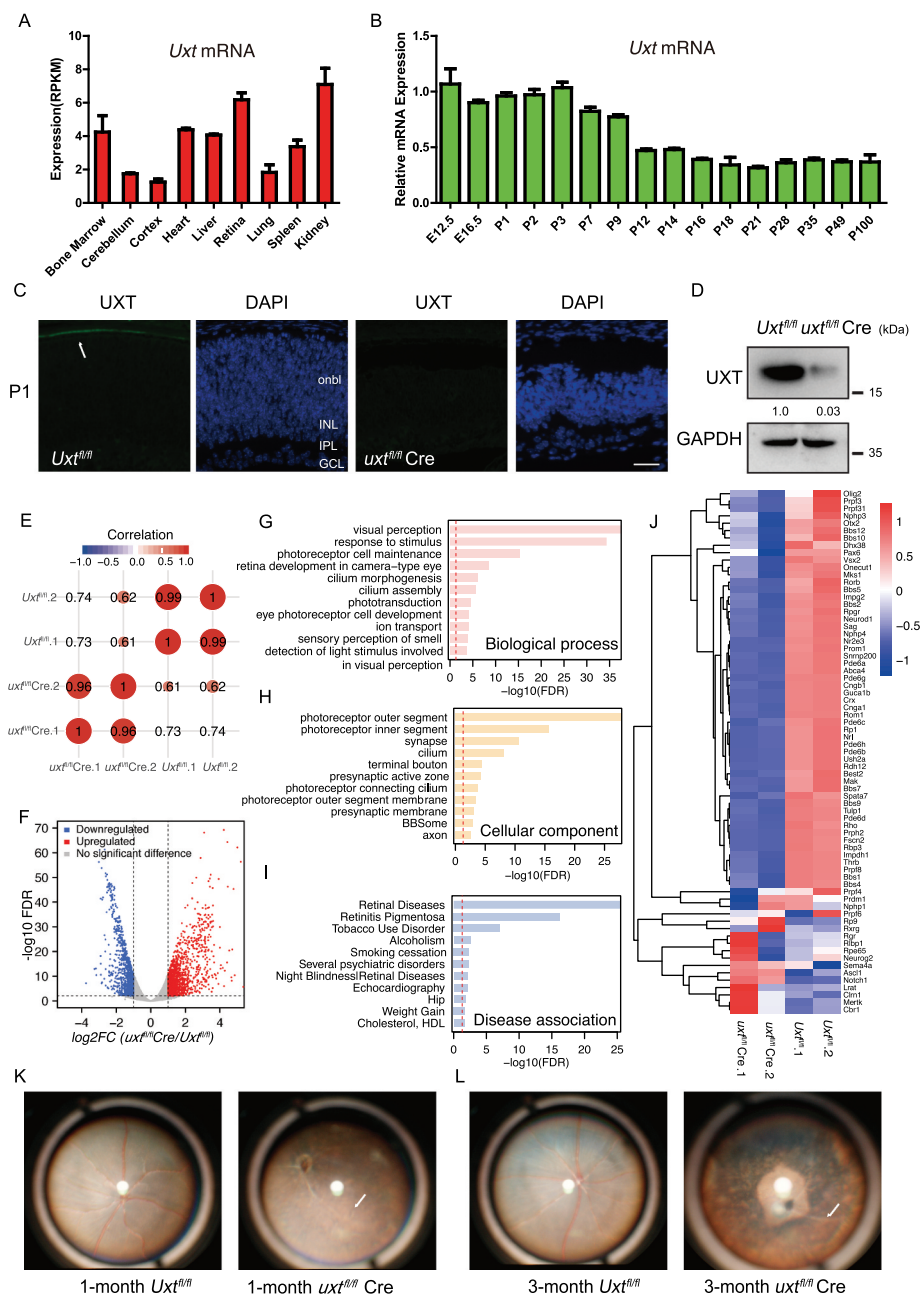


Figure 1. UXT is associated with retinitis pigmentosa. (A) Expression abundance of *Uxt* mRNA across nine mouse tissues estimated using RNA-seq data. (B) Real-time PCR analysis of *Uxt* mRNA in wild-type retinas at E12.5 (Embryo), E16.5, P1, P2, P3, P7, P9, P12, P14, P16, P18, P21, P28, P35, P49, P100. Graphs show the mean \pm SEM, and the data shown are representative of three retinas. (C) Section immunofluorescence on wild-type retinas at P30. Arrows indicate UXT proteins. Scale bars: 50 μ m. (D) Retinas were isolated from control and *uxt* KO mice at P30. Tissue homogenate was collected for western blot analysis using an anti-UXT antibody to confirm UXT ablation in the *uxt* KO retina. (E) The pairwise gene expression correlation between control (*Uxt^{fl/fl}.1* and *Uxt^{fl/fl}.2*) and *uxt* CKO (*uxt^{fl/fl}.Cre.1* and *uxt^{fl/fl}.Cre.2*) mouse retinas. The size of red circle is proportional to the magnitude of expression correlation value. Each sample was pooled with a pair of retinas. (F) Differentially expressed (DE) genes in *uxt* CKO retina (FDR<0.01, absolute LFC>1). (G and H) Significantly enriched biological processes and cellular components of the downregulated DE genes (FDR<0.01). (I) Disease association result in the downregulated DE genes (FDR<0.01). (J) The heatmap of expression changes of retinitis pigmentosa-related genes between control and *uxt* CKO retina. For each gene, the expression level was normalized (Z-score) across samples. (K and L) Retinopathy conditions measured using fundus photograph in retinas of 1-month-old and 3-month-old *uxt* CKO mice, respectively. Arrows indicate retinal degeneration and pigmentation.

P14 and P30. We recorded ERG responses with various stimulus intensities under the dark- and light-adapted conditions. Under the dark-adapted condition, the amplitude of the ERG a-waves and b-waves for *uxt* CKO mice was significantly lower than that for control mice, indicating decreased rod-mediated activity in *uxt* CKO mice

(Figure 2A and C). As for light-adapted ERG responses, the amplitude of the ERG response was dramatically decreased in *uxt* CKO mice than control mice in b-wave test and a-wave test, revealing impairments in cone function (Figure 2B and D). Collectively, *uxt* CKO mice displayed severely impaired retinal function.

Conditional knockout of *Uxt* causes specific and progressive photoreceptor cell loss leading to severe retina degeneration

We further examined retina morphology changes during retinogenesis in *uxt* CKO mice. Hematoxylin and eosin staining of control and *uxt* CKO littermates were performed at P1, P7, P14, and P30, respectively. The result showed that morphology changes of *uxt* CKO retinas occurred progressively (Figure 3A–D). The retinas of *uxt* CKO mice have a visible laminar organization at P1 and P7. At P14, morphology of *uxt* CKO retinas appeared to be severely disrupted. The defect is so severe that morphology of *uxt* CKO retinas was barely observable at P30. We further quantified the progression of the observed morphology changes by measuring the thickness and cell count of *uxt* CKO retinas (Fig. S2A and S2B). Comparing with control mice, a gradual reduction of the thickness of whole retina was detected in *uxt* CKO mice, corresponding to ~40%, ~70% and ~85% thickness reduction at P1, P7 and P14, respectively. The thickness was barely measurable at P30 in *uxt* CKO mice. Consistently, we also observed a continuing decrease in cell count in *uxt* CKO retinas. These data suggested that conditional ablation of UXT caused severe developmental defects in retina, leading to retinal degeneration in a progressive manner.

During mouse embryonic retinogenesis, retinal ganglion cells (RGCs) are generated first, followed by cone photoreceptors, rod photoreceptors and other cell types until completing differentiation. To investigate whether knockout of *Uxt* caused retina degeneration in all types of retinal cells or a cell type-specific manner, we conducted real-time PCR experiments to measure expression changes of cell type markers of seven major retina cell types in *uxt* CKO retinas, including ganglion cell markers (RBPMS, NEFL and ISL1), cone photoreceptor cell markers (OPN1SW/S-OPSIN and OPN1MW/M-OPSIN), rod photoreceptor cell markers (GNAT1 and RHO), horizontal cell marker (ONECUT2), bipolar cell markers (VSX2 and PRKCA [protein kinase C alpha]), amacrine cell marker (STX1 [syntaxin 1]) and Müller cell markers (SOX9 and VIM [vimentin]) (Figure 3E, F, S2C and S2D). We observed specific expression reduction of cell type markers of cone and rod photoreceptors at P1 and P7 while other cell type markers' expression level largely unchanged between control and *uxt* CKO retinas (Figure 3E and 3F). At P14 and P30, the expression of all cell type markers was decreased and the cell markers of photoreceptors displayed the most significant downregulation magnitude (Fig. S2C and S2D). Taken together, these results demonstrated that *uxt* CKO retina exhibited progressive photoreceptor loss, which may lead to the observed severe defects in retinal morphology and function.

A progressive alteration of retinitis pigmentosa-related gene expression in *uxt* CKO retina

The observed gradual degeneration of *uxt* CKO retina mimics the symptom of retinitis pigmentosa. To further investigate the association between the defects in *uxt* CKO retina and retinitis pigmentosa, we examined the dynamic expression changes of retinitis pigmentosa-related genes in *uxt* CKO

retinas at P1, P7, P14, and P30 by using RNA-seq (Figure 4A–E). In line with the morphology changes, the expression dysregulation of retinitis pigmentosa-related genes also occurred progressively and exhibited a global downregulation at P30. Notably, such pervasively impaired expression of retinitis pigmentosa-related genes happened as early as P14, which is similar to the observation that severe morphology abnormality in *uxt* CKO retinas initially appeared at P14. We further focused on the expression changes of major causative genes for retinitis pigmentosa such as *Rp1*, *Rho*, *Prph2*, *Prpf31*, and carried out real-time PCR to validate the expression changes of these major causative genes expression between *uxt* CKO and control retinas at P1, P7, P14 and P30. In agreement with the RNA-seq data, there is a significant decrease in the expression of *Rp1*, *Rho*, *Prph2*, *Prpf31*, *Nr2e3*, *Crx* in the *uxt* CKO retinas at all four developmental stages (Figure 4F–I). Collectively, these results demonstrated that coordinated changes occurred between the dysregulation of retinitis pigmentosa-related genes and retina morphology abnormality in *uxt* CKO retinas, suggesting that the ablation of UXT was associated with the expression reduction of the predominant retinitis pigmentosa-related genes, and thus may be a crucial target for retinitis pigmentosa.

Photoreceptors in *uxt* CKO retinas undergo apoptotic cell death

In *uxt* CKO retinas, photoreceptor cells exhibited the most dramatic degeneration. Previous studies on retinitis pigmentosa revealed apoptosis was the converging pathway of photoreceptor death in retinal degeneration [18]. To determine whether the photoreceptor loss in *uxt* CKO retinas was due to apoptosis, we performed the terminal deoxynucleotidyl transferase-mediated dUTP nick-end labeling (TUNEL) assay. The number of TUNEL-positive cells was significantly increased in *uxt* CKO retinas compared to controls at P1 and P14 (Figure 5A and C). To further confirm this, western blot was performed to measure CASP3 and PARP activity in *uxt* CKO and control retinas. We observed a strong appearance of cleaved CASP3 and PARP at P1 and P14 (Figure 5B and D). In line with these observations, a significantly higher proportion of annotated genes involved in apoptosis process was increased in *uxt* CKO retina (Figure 5E) (Fisher's exact test, $p < 0.01$). Furthermore, similar result was observed for the genes involved in promoting apoptosis while genes involved in inhibiting apoptosis displayed the opposite expression pattern (Figure 5F and G) (Fisher's exact test, $p < 0.01$). These observations indicate that apoptotic cell death may lead to loss of photoreceptors in *uxt* CKO retina.

Next, we explored whether the lack of UXT caused photoreceptor apoptotic cell death. We transfected siRNA targeting *Uxt* into mouse photoreceptor cell line 661 W (derived from murine retina photoreceptors) and measured the abundance of apoptosis-related markers. The siRNA transfection achieved knockdown of UXT efficiently (Figure 5H). In 661 W cells, depletion of UXT also resulted in increased levels of cleaved CASP3 and PARP (Figure 5I). To further confirm this, we performed real-time PCR to detect the expression level of another three master regulators of apoptosis involving in

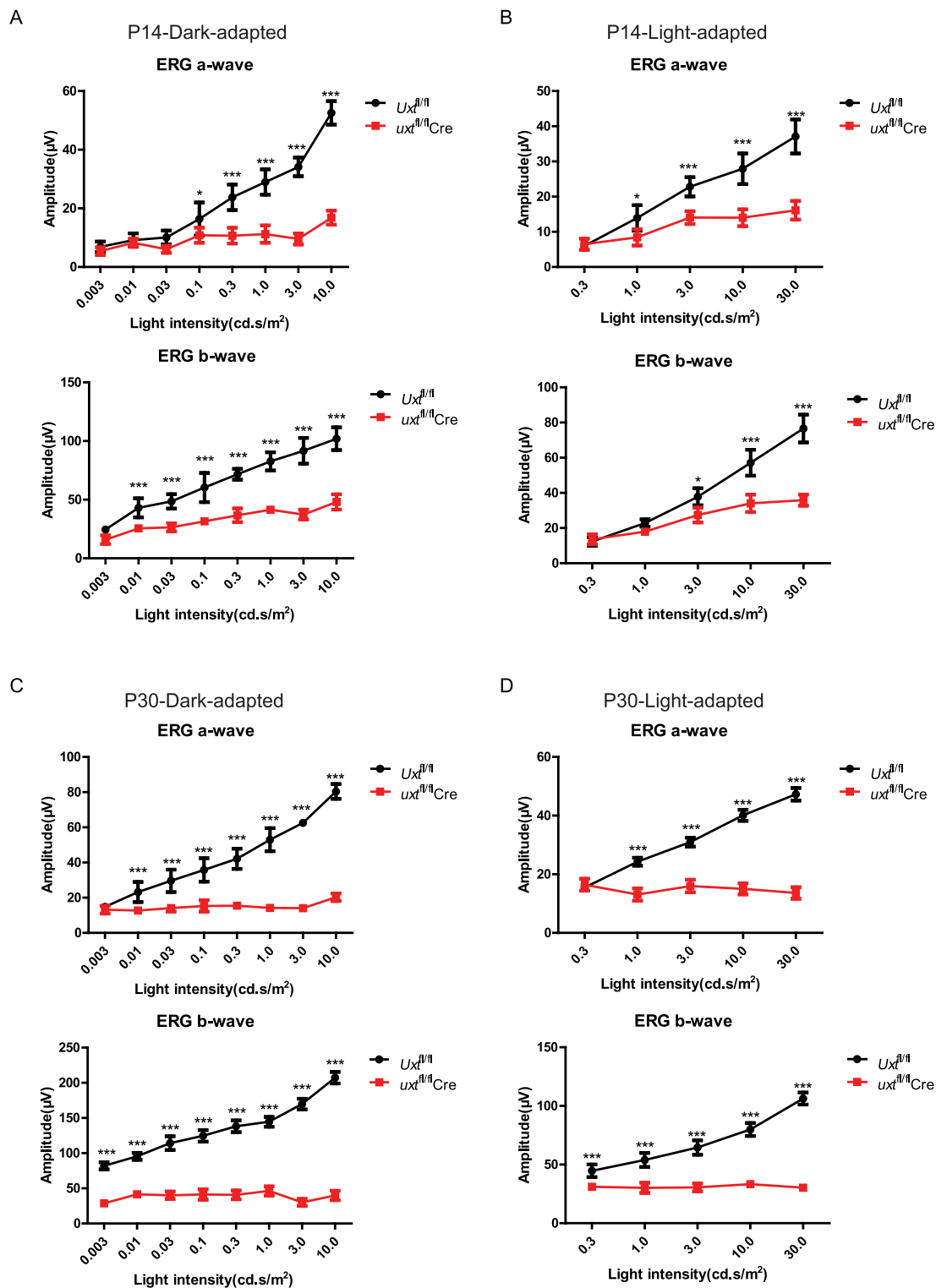


Figure 2. Impaired ERG responses in the *uxt* CKO mice. (A and C) Amplitudes of ERG dark-adapted a-waves and b-waves elicited from control and *uxt* CKO mice at P14 and P30. (B and D) Amplitudes of ERG light-adapted a-waves and b-waves elicited from control and *uxt* CKO mice at P14 and P30. Differences between control and *uxt* CKO animals are significant at all flash intensities. Graphs show the mean \pm SEM, and the data shown are representative of ten mice. *** $p < 0.001$ (Wilcoxon-Mann-Whitney test).

determining cell death fate, including BCL2 (anti-apoptotic), BAX and BAK1 (proapoptotic) [19,20]. Consistently, *Bax* and *Bak1* mRNA levels were increased while *Bcl2* mRNA level was decreased after depletion of UXT (Figure 5). These observations further confirmed the negative role of UXT in determining apoptotic cell death in photoreceptor.

The retinas of *uxt* CKO mice show enhanced autophagic flux

Previous studies have demonstrated autophagy initiates apoptosis and contributes to photoreceptor death [8,21]. Intriguingly, we found the upregulated DE genes in *uxt*

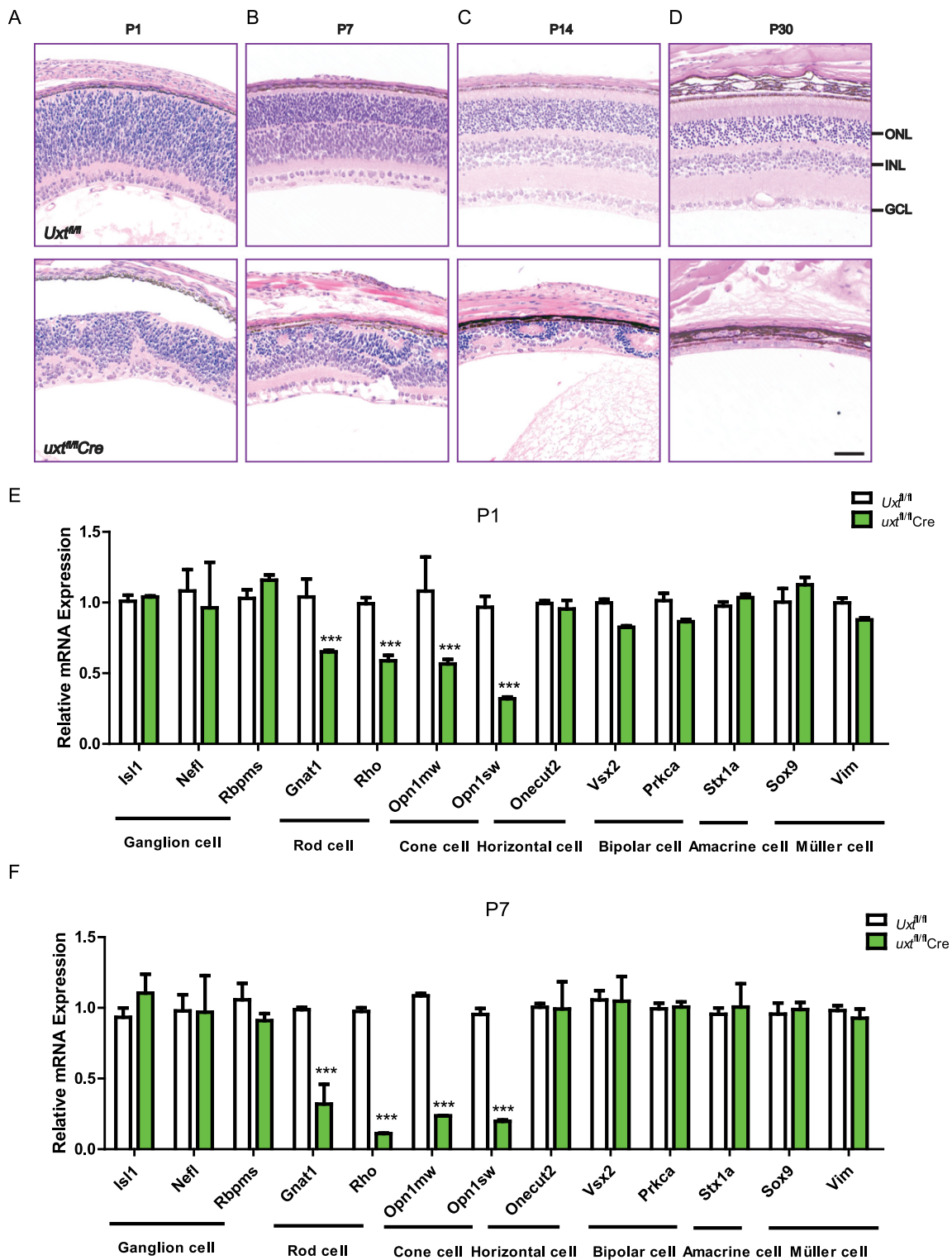


Figure 3. Conditional knockout of UXT causes severe retinal defects and progressive photoreceptor degeneration. (A, B, C and D) H&E staining of control and *uxt* CKO retinal sections from P1, P7, P14 and P30 mice. Scale bars: 50 μ m. The data shown are representative of three retinas. (E and F) Real-time PCR analysis of *Isl1*, *Nefl*, *Rbpms*, *Rho*, *Gnat1*, *Opn1sw*, *Opn1mw*, *Onecut2*, *Vsx2*, *Prkca*, *Stx1a*, *Sox9*, *Vim* mRNA in control and *uxt* CKO retinas at P1 and P7. Graphs show the mean \pm SEM, and the data shown are representative of three retinas. ***p < 0.001 (Wilcoxon-Mann-Whitney test).

CKO retina were significantly enriched in the biological process of autophagy (Fisher's exact test, FDR < 0.01). Indeed, the majority of autophagy-related genes and especially those involved in positive regulation of autophagy process were significantly increased in *uxt* CKO retina (Figure 6A and B). By contrast, the negative regulators of autophagy process were

mostly inhibited (Figure 6C). These observations made us wonder if the *uxt* CKO-induced apoptotic cell death in photoreceptor was due to overactivation of autophagy. To explore this possibility, we examined the autophagic flux in *uxt* CKO retinas by determining the abundance of SQSTM1, a well-characterized autophagy gene that is elevated after autophagy

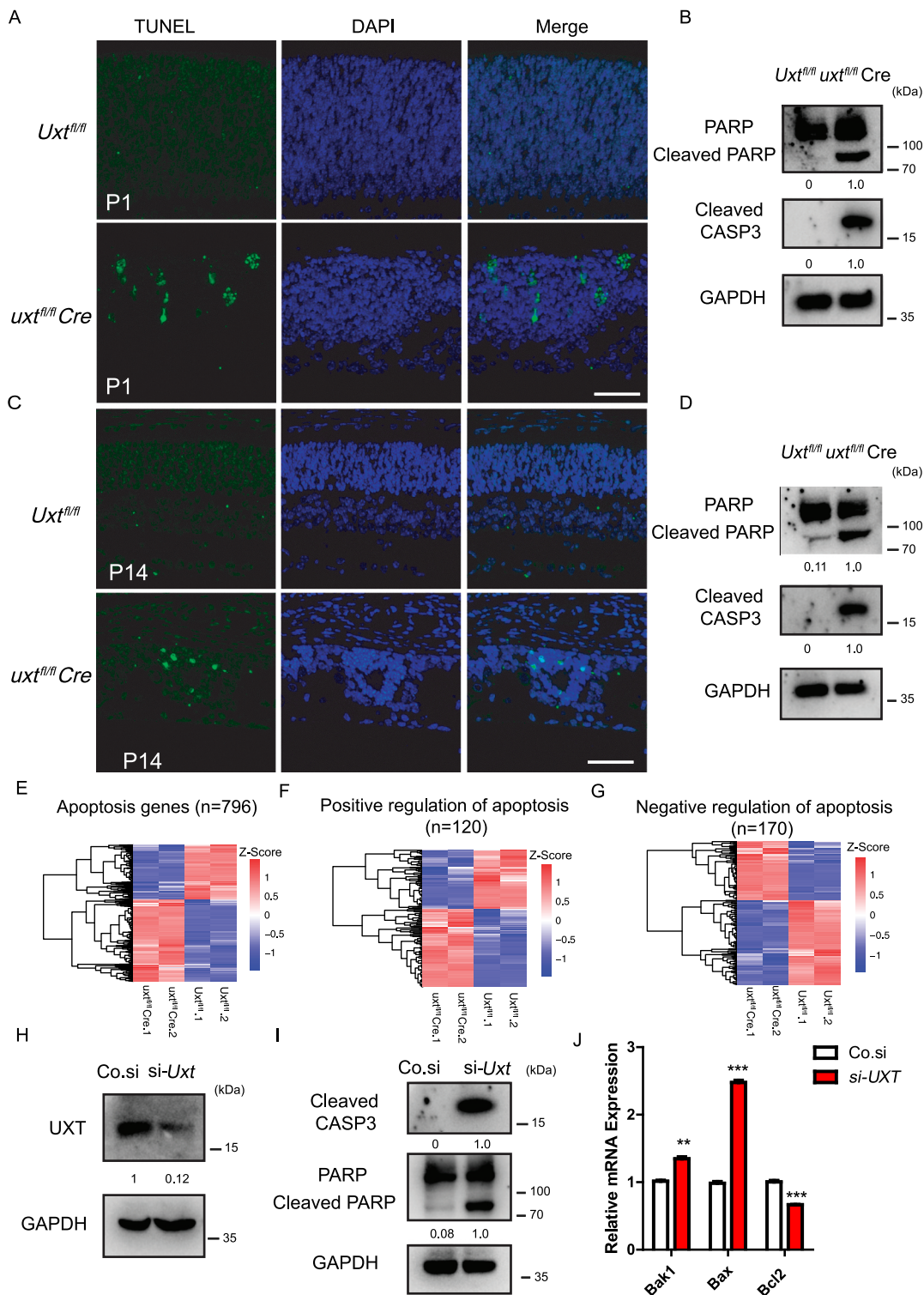


Figure 5. Photoreceptors in *uxt* CKO retinas undergo apoptotic cell death. (A) TUNEL staining of control and *uxt* CKO retinas at P1. Scale bars: 50 μ m. The data shown are representative of three retinas. (B) Retinas were isolated from control and *uxt* CKO mice at P1. Tissue homogenate was collected for western blot analysis using anti-PARP and cleaved CASP3 antibodies. (C) TUNEL staining of control and *uxt* CKO retinas at P14. Scale bars: 50 μ m. The data shown are representative of three retinas. (D) Retinas were isolated from control and *uxt* CKO mice at P14. Tissue homogenate was collected for western blot analysis using anti-PARP and cleaved CASP3 antibodies. (E, F and G) The heatmap of gene expression changes between control and *uxt* CKO retina from apoptosis genes, positive regulation of apoptosis genes and negative regulation of apoptosis genes categories, respectively. For each gene, the expression level was normalized (Z-score) across samples. (H) 661 W cells were transfected with the indicated siRNAs. Cell lysates were collected for western blot analysis of UXT and GAPDH. (I) 661 W cells were transfected with the indicated siRNAs. Cell lysates were collected for western blot analysis of PARP, cleaved CASP3 and GAPDH. (J) 661 W cells were transfected with the indicated siRNAs. The alternation of *Bak1*, *Bax*, *Bcl2* mRNAs was measured by real-time PCR. Graphs show the mean \pm SEM, and the data shown are representative of three independent experiments. ** $p < 0.01$; *** $p < 0.001$ (Wilcoxon-Mann-Whitney test).

result showed that LC3-II was significantly increased in *uxt* CKO retinas (Figure 6E and G). This observation further confirmed the elevated autophagy flux in *uxt* CKO retinas.

Next, we investigated whether depletion of UXT increased autophagic flux in photoreceptor. To check this, we transfected 661 W cells with *Uxt* siRNA and conducted real-time PCR to measure the expression changes of a group of well-established autophagy genes, including *Atg4b*, *Uvrag*, *Wip1*, *Vps11*, *Vps18*, *Atg9b* and *Tfeb*. These autophagy genes were significantly increased after knockdown of UXT (Figure 6H). Furthermore, the knockdown of UXT also resulted in decreased level of SQSTM1 and increased levels of LC3-II in 661 W cells (Figure 6I). These results consistently support elevated autophagic flux after UXT knockdown. To further confirm this, we checked autophagic flux changes after manipulating this process using specific modulators. Leupeptin has shown to suppress lysosome degradation and led to the accumulation of autolysosomes [24]. In line with the induction of autophagic flux, we detected accumulation of LC3-II after leupeptin treatment in UXT knockdown 661 W cell line (Figure 6J). 3-methyladenine (3-MA) is an inhibitor of autophagy by blocking the formation of autophagosomes [25]. We further examined whether inhibiting autophagy using 3-MA could attenuate UXT ablation induced photoreceptor apoptotic cell death. Photoreceptor apoptotic cell death was indeed suppressed after 3-MA treatment in UXT knockdown 661 W cells, along with reduced LC3-II as expected (Figure 6K). Collectively, these results revealed UXT inhibited photoreceptor cell death by regulating autophagic flux.

UXT interacts directly with MTOR and promotes MTOR activity

Finally, we investigated the mechanism underlying the UXT depletion-induced elevation of autophagic flux and cell death in photoreceptor. Among several key components of autophagy, we found TFEB was strongly enhanced in *uxt* CKO retinas and UXT knockdown 661 W cells, which is a master regulator for transcription of genes that involved in autophagy and lysosomal biogenesis [26]. The degradation of TFEB is mainly regulated by MTOR through serine phosphorylation [27]. In addition, MTOR signaling pathway plays a key role in regulating autophagy as a negative regulator [9], which has been demonstrated to be involved in regulating photoreceptor cell death in experimental RP model [11]. We wondered whether UXT could interact with MTOR and thus regulate MTOR activity. To explore this possibility, we ectopically expressed UXT and MTOR in HEK293T cells, and then tested the interactions between them. Interestingly, UXT could directly interact with MTOR (Fig. S3A and S3B). Importantly, we further confirmed the endogenous interaction between UXT and MTOR in both mouse retina and 661 W cells (Figure 7A and B).

Then, we went on to examine MTOR activity after the ablation of UXT. RPS6KB1/S6K, a substrate of MTOR, is phosphorylated and activated by MTOR [28]. Moreover, RPS6KB1 is critical for both rod and cone survival in rd10 mice [29]. Therefore, we measured the phosphorylation level of RPS6KB1 as a proxy to estimate MTOR activity. Decreased

phosphorylation level of RPS6KB1 was observed in *uxt* CKO retinas (Figure 7C, 7D, S3C and S3D). Furthermore, the knockdown of UXT using siRNA also led to impaired phosphorylation level of RPS6KB1 in 661 W cells (Figure 7E). These observations suggested that UXT could interact with MTOR and promote MTOR activity.

Torin1 is an effective and selective inhibitor of MTOR [30]. Therefore, we further examined the functional dependency of UXT on MTOR by first silencing MTOR activity using torin1. Similar to the observations in UXT knockdown photoreceptor cells and *uxt* CKO retina, treatment of torin1 increased levels of cleaved CASP3 while not affecting MTOR expression level in 661 W cell (Figure 7F and S3E). In addition, *Bax* and *Bak1* mRNA levels were increased while *Bcl2* mRNA level was decreased after torin1 treatment (Figure 7G). Notably, UXT overexpression could not affect the levels of apoptotic markers after the inhibition of MTOR by torin1, demonstrating that the function of UXT in photoreceptor cells was dependent on MTOR (Figure 7H and I). Collectively, these results revealed a critical role of UXT in regulating MTOR activity in photoreceptor cells.

Discussion

In this study, we uncovered a vital role of UXT in preventing retina from degeneration. The mice deficient in UXT displayed severe retina defects at molecular, morphological and functional aspects. Based on ERG and fundus photography experiments, we observed severely affected retinal structure and function in *uxt* CKO retinas. These morphological and functional abnormalities were accompanied by the specific and progressive reduction of photoreceptor cells as well as the gradual dysregulation of genes involved in normal photoreceptor function and retinitis pigmentosa, which recapitulated the key features of retinitis pigmentosa.

Retinitis pigmentosa is the most common hereditary retinopathy from various gene mutations causing bilateral blindness. The detailed mechanisms that cause progressive loss of photoreceptors are still largely unknown. Autophagy and oxidative stress are implicated in retinitis pigmentosa [6]. Comparing with control mice, we found that autophagic flux was significantly enhanced in *uxt* CKO retinas. This result suggests overactivation of autophagy may contribute to the observed retinitis pigmentosa-like phenotype in *uxt* CKO retinas, which is in line with the previous observation that autophagy may initiate apoptosis and further contribute to photoreceptor death [8]. It should be noted that autophagy seems to play a dual role in affecting cell death and retinal degeneration. Previous studies suggested low level of stress might be beneficial while high level of stress caused detrimental effects that resulted in increased cell death and retinal degeneration [31]. In addition, it has been reported the deletion of *Atg5*, an essential protein in the cascade of autophagy, causes a decrease in autophagy and induced cell death of rod cells [32,33]. The role of autophagy in retinitis pigmentosa seems to be context-dependent and detailed mechanisms still require further exploration.

The MTOR pathway plays an essential role in cell metabolism, survival and growth [34–36]. Aberrant MTOR activation

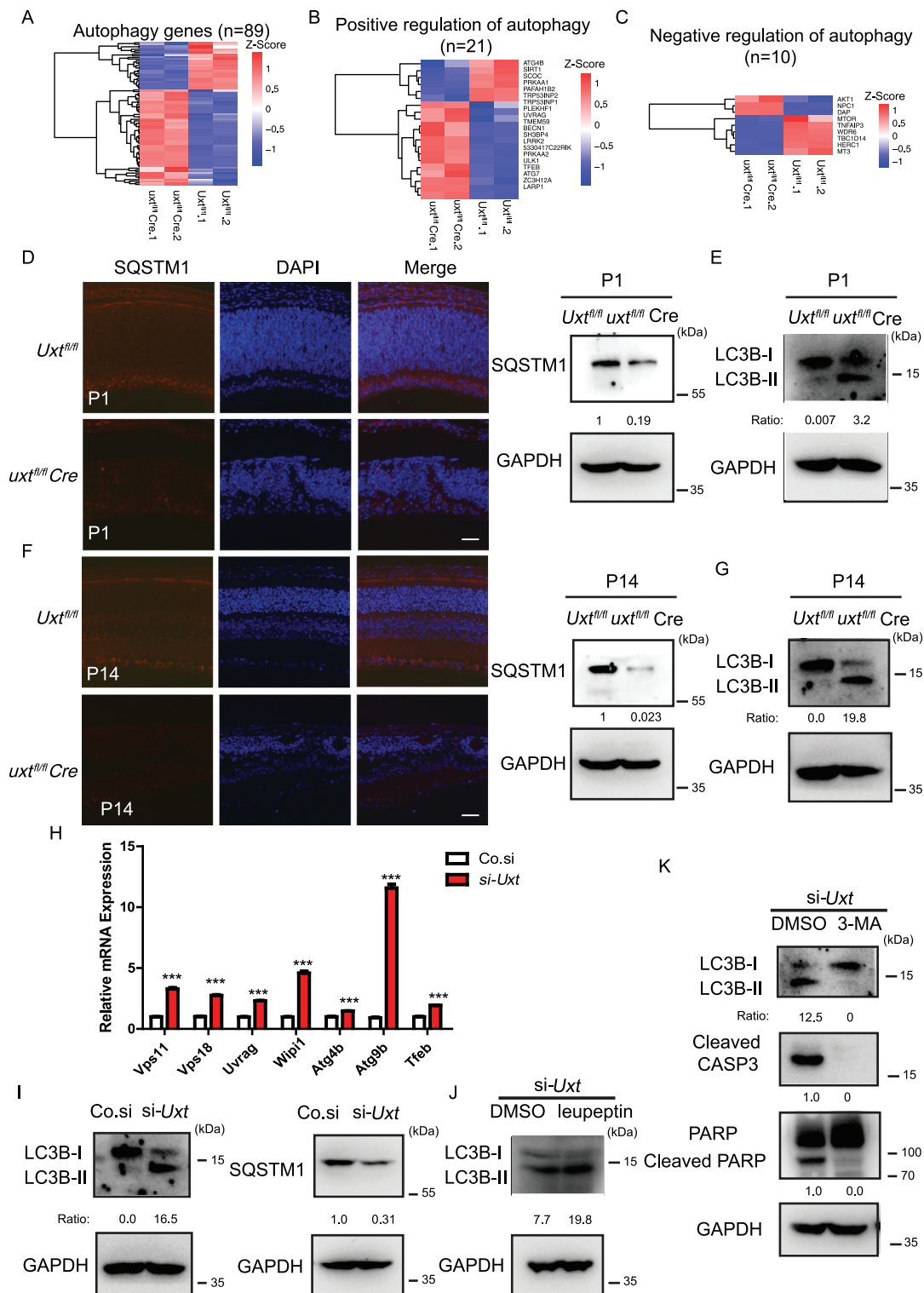


Figure 6. The retinas of *uxt* CKO mice show enhanced autophagic flux. (A, B and C) The heatmap of gene expression changes between control and *uxt* CKO retina from autophagy genes, positive regulation of autophagy genes and negative regulation of autophagy genes categories, respectively. For each gene, the expression level was normalized (Z-score) across samples. (D) Immunostaining and western blot analysis of SQSTM1 in the retinas of control and *uxt* CKO retinas at P1. Scale bars: 50 μ m. The data shown are representative of three retinas. (E) Retinas were isolated from control and *uxt* CKO mice at P1. Tissue homogenate was collected for western blot analysis using anti-LC3B and GAPDH antibodies. (F) Immunostaining and western blot analysis of SQSTM1 in the retinas of control and *uxt* CKO retinas at P14. Scale bars: 50 μ m. The data shown are representative of three retinas. (G) Retinas were isolated from control and *uxt* CKO mice at P14. Tissue homogenate was collected for western blot analysis using anti-LC3B, SQSTM1 and GAPDH antibodies. (H) 661 W cells were transfected with the indicated siRNAs. The alternation of *Atg4b*, *Uvrag*, *Wip1*, *Vps11*, *Vps18*, *Atg9b* and *Tfeb* mRNAs was measured by real-time PCR. Graphs show the mean \pm SEM, and the data shown are representative of three independent experiments. *** $p < 0.001$ (Wilcoxon-Mann-Whitney test). (I) 661 W cells were transfected with the indicated siRNAs. Cell lysates were collected for western blot analysis of LC3B, SQSTM1 and GAPDH. (J) 661 W cells were transfected with the indicated siRNA for 24 h. Then, 661 W cells were treated with 10 μ g/ml leupeptin for 24 h. Cell lysates were collected for western blot analysis of LC3B and GAPDH. (K) 661 W cells were transfected with the indicated siRNA for 24 h. Then, 661 W cells were treated with 500 nm/ml 3-MA for 24 h. Cell lysates were collected for western blot analysis of LC3B, PARP, cleaved CASP3 and GAPDH.

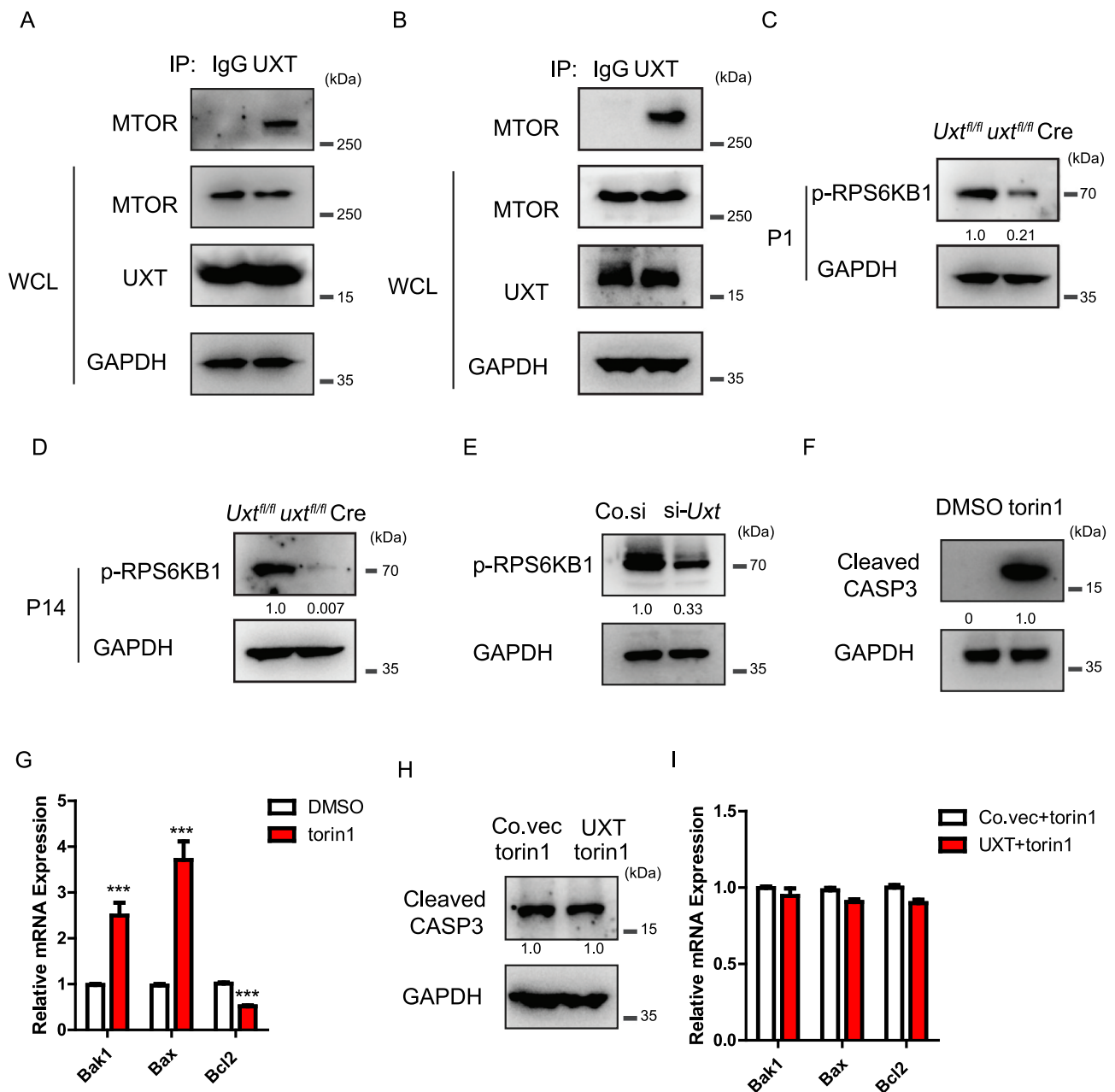


Figure 7. UXT interacts directly with MTOR and functions as a partner of MTOR. (A) Lysates of retinas were immunoprecipitated with an anti-UXT antibody and then immunoblotted with the indicated antibodies. (B) Lysates of 661 W cells were immunoprecipitated with an anti-UXT antibody and then immunoblotted with the indicated antibodies. (C and D) Retinas were isolated from control and *uxt* CKO mice at P1 and P14. Tissue homogenate was collected for western blot analysis using anti-p-RPS6KB1 and GAPDH antibodies. (E) 661 W cells were transfected with the indicated siRNAs. Cell lysates were collected for western blot analysis of p-RPS6KB1 and GAPDH. (F) 661 W cells were treated with DMSO and 250 nm/ml torin1, respectively, for 48 h. Cell lysates were collected for western blot analysis of cleaved CASP3 and GAPDH. (G) 661 W cells were treated with DMSO and 250 nm/ml torin1, respectively, for 48 h. The alteration of *Bak1*, *Bax*, *Bcl2* mRNAs was measured by real-time PCR. (H) 661 W cells were transfected with the indicated plasmid for 24 h. Then, 661 W cells were treated with 500 nm/ml torin1 for 24 h. Cell lysates were collected for western blot analysis of cleaved CASP3 and GAPDH. (I) 661 W cells were transfected with the indicated plasmid for 24 h. Then, 661 W cells were treated with 500 nm/ml torin1 for 24 h. The alteration of *Bak1*, *Bax*, *Bcl2* mRNAs was measured by real-time PCR. Graphs show the mean \pm SEM, and the data (G and I) shown are representative of three independent experiments. *** $p < 0.001$ (Wilcoxon-Mann-Whitney test).

has been demonstrated to be involved in many disorders, like neurological diseases [37,38]. Recent studies revealed that MTOR functions to promote photoreceptor survival in mouse RP models [10,11]. Moreover, RPS6KB1, a downstream factor of MTOR, plays an important role in both rod and cone survival in *rd10* mice [29]. In addition, the genes involved in regulating MTOR have been reported to modulate cone cell death [39,40]. These observations

demonstrated a strong association between MTOR pathway and normal photoreceptor function. Importantly, our study found that UXT was indispensable in regulating MTOR activity. We identified a direct interaction between UXT and MTOR in mouse retina and photoreceptor cells. Loss of UXT strongly impaired MTOR activity. Considering the tight associations between MTOR and autophagy, our results indicate loss of UXT impaired MTOR activity, which in turn

led to increased autophagy flux and apoptosis along with pervasive reduction of photoreceptor cells and downregulation of retinitis pigmentosa-related genes, finally resulting in severe retina degeneration and abnormal retina function. Although our study uncovered the importance of MTOR as an essential upstream regulator of increased autophagic flux in *uxt* CKO retina, it should be noted that autophagy is an elaborate and sophisticated process that is under tight surveillance of other crucial modulators. Therefore, probing more detailed and comprehensive mechanisms underlying the profound effect of *Uxt* deletion in retina is still an intriguing question requiring further exploration.

In terms of pathology and disease progression, typical RP patients lose night vision in adolescence, side vision in young adulthood, and central vision in later life due to the progressive loss of rod and cone photoreceptor cells [41]. However, RP is a highly heterogeneous retinopathy. Some patients may have developed severe systematic visual loss in childhood, while others may remain asymptomatic even in mid-adulthood [41]. Such big heterogeneity in pathology is not that unexpected since, by definition, RP is the term given to a set of retinal diseases that only share degeneration features of rod and cone photoreceptors. Many clinical assessments have been applied to diagnose RP, in which ERG is a kind of objective measurement of retinal function for accurate disease diagnosis and severity assessment [42]. In *uxt* CKO mice retina, the ERG responses were dramatically impaired at both P14 and P30. Moreover, we also observed other histological and physiological defects in *uxt* CKO mouse retina similar to that of RP including progressive loss of photoreceptor cells as well as more severe hyperpigmentation in 3-month-old *uxt* CKO mouse retina than that of 1-month-old *uxt* CKO mouse retina. At molecular level, we detected concordant expression alteration including significant alterations of retinitis pigmentosa-related genes in *uxt* CKO mouse retina. The pervasive expression changes of canonical retinitis pigmentosa-related genes were progressed in a continuing matter, and finally led to excessive expression reduction globally. All these observations indicated *uxt* CKO mice exhibit similar features of RP at molecular, morphological and functional aspects. However, one notable difference between the phenotype of *uxt* CKO mice and that of typical RP patients is that the retinal degeneration progressed more rapidly in UXT-deficient mice, which might rarely be observed in typical RP patients. Because of the rapid retinal degeneration, we measured molecular, histological, and morphological changes during youth developmental stages at P1, P7, and P14 to access pathological progress. Such relatively fast retinal degeneration pathological progress was possibly due to the excessive reduction of multiple retinitis pigmentosa causal genes that might function synergistically to greatly accelerate pathological progress in *uxt* CKO mice. Intriguingly, UXT is a protein-coding gene located on chromosome X. Previous studies have shown that X-linked RPs usually have an early age of onset and are generally more severe in pathology [43]. Although the X chromosome location might be a coincidence, it might still be possible that other unknown factors work along with the factor of X chromosome location to accelerate RP pathological progress in *uxt* CKO mice. Mouse models of retinitis

pigmentosa, such as rd1-10, have been investigated for many years [44]. In our opinion, *uxt* CKO mice may belong to a novel X-linked atypical RP mouse model, or alternatively, represent a kind of RP-like mouse model. It also should be noted that the relatively fast pathological progress might obstruct a more general application of our RP-like mouse model. However, the potential positive aspect is that *uxt* CKO mice may allow researchers to test the effects of anti-RP treatments or therapies faster in terms of RP phenotype observation, compared to the RP models that have relatively late age of onset and slower pathological progress.

Taken together, our study reveals a crucial role of UXT in promoting MTOR activity to prevent retina from degeneration. UXT is necessary for the normal function and integrity of mouse retina, the ablation of which was associated with pervasive reduction of genes required for photoreceptor cell development and phototransduction within photoreceptor segment. Loss of UXT was associated with significant alteration of retinitis pigmentosa-related genes. Therefore, UXT-deficient mice could serve as a potential disease-model for retinal degenerative diseases, which is instrumental for elucidating and further manipulating photoreceptor degeneration in future studies. The identification of UXT may provide a candidate gene for the site of mutations responsible for retinal degenerative disease. Hopefully, UXT is a potential candidate for targeting retinal degenerative diseases.

Materials and Methods

Mice

C57BL/6 mice were purchased from the Model Animal Research Center of Nanjing University. The mice were maintained under specific pathogen-free (SPF) conditions at the Center for New Drug Safety Evaluation and Research, China Pharmaceutical University. The *uxt* conditional knockout mice were generated by mating between *Vsx2-Cre* and *uxt^{fllox/fllox}* mice. *Vsx2-Cre* mice were purchased from Shanghai Biomodel Organism. *Uxt* flox mice were generated with CRISPR-Cas9-mediated homologous recombination of a 2,289 bp double-stranded DNA donor containing two loxP sites flanking exon 3. The donor DNA was prepared by two steps of fusion PCRs using C57/BL6 genomic DNA as template and an EcoRI site was incorporated 5' to the loxP site. The final donor DNA contained a floxed region (containing exon 3) of 242 bp by two EcoRI-loxP sites (40 bp each) and two homology arms of 980 bp and 987 bp, respectively. Two guide RNAs targeting the intron 2 (5'-GATGCCAGGCATTTTAAAGTC-3') and intron 3 (5'-GTGTCAGCGGGCAATTTTAA-3') were designed using the Zhang Lab CRISPR tool (<http://crispr.mit.edu/>). The two sgRNAs and *Cas9* mRNA were *in vitro* transcribed, mixed and injected into the cytoplasm and pronucleus of C57/BL6 fertilized eggs. Founders were screened by PCR genotyping using primers: forward, 5'-CATGTCAACCACAACCTGAC-3' and reverse, 5'-TAGGTGTCAGCGGGCAATTT-3', and confirmed by long-range PCR, EcoRI digestion and Sanger sequencing. All genotypes were determined by PCR using

a T5 Direct PCR Kit (Tsingke, TSE012). These strains were maintained on a C57BL/6 background. Age-matched *Uxt^{fllox}* mice were used as a control. All animal experiments were performed in accordance with the National Institutes of Health Guide for the Care and Use of Laboratory Animals. The protocol was approved by the Institutional Animal Care and Use Committee of China Pharmaceutical University and the Institutional Ethics Committee of China Pharmaceutical University (Approval Number 2020-01-002).

Cell culture

The HEK293T cell line was obtained from the American Type Culture Collection (ATCC, CRL-3216). The 661 W cell line was a gift from Dr. Xin Zhang (The First School of Clinical Medicine, Nanjing Medical University). HEK293T and 661 W cell lines were maintained in Dulbecco's modified Eagle's medium (Thermo Fisher Scientific, 11210006; DMEM) containing 10% fetal bovine serum (Thermo Fisher Scientific, 12484028; FBS) under a humidified atmosphere of 5% CO₂ at 37°C. Cultured cells were released by trypsin and passaged every 2 d.

Antibodies and reagents

Torin1 (SC0245) was purchased from Beyotime Biotechnology. Leupeptin (HY-18234A) and 3-MA (HY-19312) were purchased from MedChemExpress. The following antibodies were used: anti-UXT (Invitrogen, PA5-18852), anti-HA (Santa Cruz Biotechnology, sc-7392), anti-FLAG (Santa Cruz Biotechnology, sc-8036), anti-cleaved CASP3 (Cell Signaling Technology, 9664S), anti-PARP (Cell Signaling Technology, 9532S), anti-GAPDH (Santa Cruz Biotechnology, sc-32233), anti-LC3B (Cell Signaling Technology, 3868S), anti-MTOR (Cell Signaling Technology, 2972S), anti-SQSTM1 (Cell Signaling Technology, 23214S), normal mouse IgG (Santa Cruz Biotechnology, sc-2025), normal rabbit IgG (Santa Cruz Biotechnology, sc-2027), normal goat IgG (Santa Cruz Biotechnology, sc-2028), anti-p-RPS6KB1/S6K (Cell Signaling Technology, 2708S).

Real-time PCR

Total cellular RNA was isolated using Trizol (Invitrogen, 1596018) according to the manufacturer's instructions, then reverse transcription was performed using a reverse transcription kit (Vazyme, R223-01). The quantification of gene transcripts was performed by real-time PCR using SYBR Green PCR mix (Vazyme, Q331-02/03). All values were normalized to the level of *Gapdh* mRNA. The primers used were listed below:

Gapdh, sense (AGGTCGGTGTGAACGGATTG), antisense (TGTAGACCATGTAGTTGAGGTCA);
Opn1sw, sense (CAGCCTTCATGGGATTTGTCT), antisense (CAAAGAGGAAGTATCCGTGACAG);
Opn1mw, sense (ATGGCCCAAAGGCTTACAGG), antisense (AAGGGACCTTTGGTGCTGTT);
Rho, sense (CCCTTCTCCAACGTCACAGG), and antisense (TGAGGAAGTTGATGGGGAAGC);

Gnat1, sense (GGATGGCTACTCACCCGAAG), antisense (TGCATAGTCAATGCCTAGTGTG);
Isl1/Islet1, sense (ATGATGGTGGTTTACAGGCTAAC), antisense (TCGATGCTACTTCACTGCCAG);
Onecut2, sense (GGCTTCCGTCCATGAACAAC), antisense (CGAAATTGGGGCTGAGCATTFTT);
Vsx2, sense (CTGAGCAAGCCCAAATCCGA), antisense (CGCAGCTAACAAATGCCAG);
Stx1a, sense (AGAGATCCGGGGCTTTATTGA), antisense (AATGCTCTTTAGCTTGGAGCG);
Vim, sense (CGGCTGCGAGAGAAATTGC), antisense (CCACTTTCCGTTCAAGGTCAAG);
Sox9, sense (CGGAACAGACTCACATCTCTCC), antisense (GCTTGCACGTCGGTTTTGG);
Rbpms, sense (CCCGTAGGCTTTGTGAGTTTT), and antisense (GTAAAGTGCAGGTACTGTGAGC);
Prkca, sense (GTTTACCCGGCCAACGACT), and antisense (GGGCGATGAATTTGTGGTCTT);
Bax, sense (TGAAGACAGGGGCTTTTTTG), antisense (AATTCCGGGAGACACTCG);
Bak1, sense (CAACCCCGAGATGGACAACCTT), antisense (CGTAGCGCCGGTTAATATCAT);
Vps11, sense (CACAGGAAGTGGACTGAGGG), and antisense (CAGGAAATCCAGGAGCTCAA);
Vps18, sense (TGGTCCAGGAACATCTTGTG), antisense (CTGGGCAAGGATACACTGCT);
Uvrag, sense (TTGCACACTGGGCTCTATGA), antisense (CATCCAAACGCACAGAAGAA);
Wipi1, sense (CTGCTTCTCTTTCAACCAAGACT), antisense (ACGTCAGGGATTTTCATTGCTT);
Atg4b, sense (GTCAAGTATGGTTGGGCAGTT), antisense (TGTCACCCTCTCCCTCGAAAT);
Atg9b, sense (CCATCCCACAATGATACACACC), and antisense (CCTCTAGCCGTTTCATAGTCTT);
Tfeb, sense (AAGGTTCCGGAGTATCTGTCTG), and antisense (GGGTTGGAGCTGATATGTAGCA);
Rp1, sense (TGACCAACAGACCTTCGGAAA), and antisense (TGATGGCAACATGCTTCAGAAC);
Prpf31, sense (GCTTCTCTTCTACCTCAGTGTG), and antisense (CATCCTTTAGTTCGTAGCCCAC);
Bcl2, sense (GTCGCTACCGTCGTGACTTC), and antisense (CAGACATGCACCTACCCAGC);
Crx, sense (GTTCAAGAATCGTAGGGCGAA), and antisense (TGAGATGCCCAAAGGATCTGT);
Nr2e3, sense (AAATGGGGCCAAAACCTTGCCT), and antisense (GAACCGGGAGATGGTTTCCTG);
Prph2, sense (CCAACAACCTCGGCGCACTA), and antisense (CCTCCGGGTTAGACACACTCT).

Western blot

Cell pellets were collected and resuspended in RIPA buffer (50 mM Tris-HCl, pH 7.4, 150 mM NaCl, 1 mM EDTA, 0.5% NP40 [Sigma-Aldrich, NP40], 0.25% Na-deoxycholate [Sigma-Aldrich, D6750], 1 mM Na₃VO₄ [Sigma-Aldrich, 450243], 0.1% SDS [Sigma-Aldrich, L3771], 0.1 mM PMSF [Sigma-Aldrich, PMSF-RO], Roche complete protease inhibitor set [Roche, 04693116001]). The resuspended cell pellet was vortexed for 20 s and then incubated on ice for 20 min, followed by

centrifugation at 10,000 \times g for 15 min. Afterward, supernatants were collected for subsequent western blot analysis. Mice retinas were homogenized with RIPA buffer and centrifuged, then supernatants were collected for subsequent western blot analysis. Protein samples were boiled for 6 min, electrophoresed in SDS polyacrylamide gel, and transferred onto PVDF membranes (Bio-Rad, 1704156). The blots were blocked with 5% BSA (Sigma-Aldrich, B2064) in Tris-buffered saline solution–Tween 0.1% (Sigma-Aldrich, P1754; TBST) for 1 h at room temperature and probed with primary antibodies at the appropriate dilutions (1:1000) overnight at 4°C. The blots were washed 5 times with TBST and incubated for 2 h at room temperature with the HRP-conjugated secondary antibody (dilution 1:5000; Sigma-Aldrich, A6154), then developed with enhanced chemiluminescence. The densitometry of protein bands was quantified by using ImageJ software (National Institutes of Health). Three separate western blots were quantified for densitometry data.

Immunoprecipitation assay

For immunoprecipitation assay, retina and cell extracts were prepared by using lysis buffer (50 mM Tris HCl, pH 7.4, 150 mM NaCl, 0.5% Triton X-100 [Sigma-Aldrich, X100], 1 mM EDTA) supplemented with a protease inhibitor cocktail (Roche, 04693116001). The lysate was incubated with appropriate antibodies for 4 h to overnight at 4°C before adding protein A/G agarose beads (Thermo Fisher Scientific, 78610) for another 2 h. The beads were washed three times with the lysis buffer and eluted with SDS-loading buffer for 5 min.

Histology, immunofluorescence and TUNEL assays

For histology, eyes from control and *uxt* CKO mice were enucleated, fixed in buffered mixed aldehydes (3% paraformaldehyde and 2% glutaraldehyde, in PBS, pH 7.4) overnight, and embedded in paraffin. Sections of 5 μ m were stained with H&E. Images were obtained with an Olympus BX41 microscope. For immunofluorescence, eyes from control and *uxt* CKO mice were enucleated, fixed in buffered 4% PFA (4% paraformaldehyde, in PBS, pH 7.4) overnight, and embedded in paraffin. Eyes were cut into 5- μ m sections. After dewaxing and rehydration, the sections were soaked in sodium citrate buffer for heat-induced epitope retrieval and incubated with 10% goat serum (Solarbio, SL038) for 1 h to block the nonspecific binding sites. Then, sections were incubated with anti-SQSTM1 (Cell Signaling Technology, 23214S; dilution 1:1000) respectively overnight at 4°C, followed by incubation with secondary antibody (dilution 1:2000) for 1 h and then stained with DAPI (Invitrogen, P36931) for 2 min. TUNEL assay was performed using the in situ Cell Death Detection Kit (Roche, 11684817910). Images were captured using a Nikon Inverted Microscope Ts2/Ts2R (Nikon ECLIPSE Ts2/Ts2R).

Plasmids, siRNA oligos, and cell transfection

Mouse *Uxt* and *Mtor* cDNA was amplified by using standard PCR techniques from mouse retina cDNA library and then sub-

cloned into the indicated vectors. The siRNA oligos were synthesized by GenePharma: *Uxt* siRNA: 5'- CCAAGGACU CCAUGAAUAUTT -3'. Cells were transfected with siRNA oligos using Lipofectamine 3000 (Invitrogen, L3000015) and then incubated for 48 h before further analysis. The plasmids were introduced into cells using Lipofectamine 3000, and then cells were cultured for 24 h before further analysis.

RNA-seq experiments and analysis

Total RNA was extracted from control and *uxt* CKO retinas using the Trizol reagent (Invitrogen, 15596018) and prepared into cDNA library according to the standard Illumina RNA-seq instruction. The generated cDNA library was sequenced in 2 \times 150 bp paired-end layout using Illumina HiSeq2500. To estimate gene expression changes between control and *uxt* CKO retinas, the raw RNA-seq data were preprocessed using Trimmomatic to remove reads in low quality and adaptor contamination [45]. The high-quality reads were further aligned to the mouse genome (mm10) using HISAT2 with default parameters [46]. The mouse genome (mm10) was downloaded from the FTP of Ensembl database [47]. We only retained uniquely mapped reads for gene expression quantification at count level using feature counts, based on mouse gene annotation of Ensembl [48]. The log₂-transformed gene expression fold-changes (LFC) and significantly differentially expressed (DE) genes were calculated using edgeR [49] after TMM normalization (FDR < 0.01, absolute value of LFC > 1). All original RNA-seq data are deposited in GEO database with accession number: GSE143281.

Functional enrichment and disease association analyses

The gene ontology (GO) enrichment analyses of up- and down-regulated DE genes between control and *uxt* CKO retinas were performed using David Bioinformatics [50]. The significantly enriched GO items of biological process (BP) and cellular component (CC) categories were selected based on intersection of the following two criteria: (1) Benjamini & Hochberg (BH) adjusted p-value < 0.01; (2) FDR < 0.01. All expressed genes in control and *uxt* CKO retinas were used as background.

The disease association analysis was performed based on the annotation of Gene-Disease Association Database (GAD). The GAD encompasses comprehensive human genetic associations by data aggregation from genome-wide association and other genetic association studies [51]. To identify significantly associated diseases for up- and downregulated DE mouse genes, we mapped mouse gene to the corresponding human ortholog strictly by retaining only one to one orthologous gene between mouse and human based on ensembl compara database [52]. We further used fisher's exact test to identify significantly associated diseases based on intersection of the following two criteria: (1) Benjamini & Hochberg (BH) adjusted p-value < 0.01; (2) FDR < 0.01.

Uxt expression level estimation in mouse tissue

To estimate *Uxt* expression abundance in different mouse tissue, we downloaded the raw RNA-seq data of GSE29184

[53] and GSE101986 from GEO [54], which covered 9 mouse tissues, including bone marrow, cerebellum, cortex, heart, liver, retina, lung, spleen and kidney. To make unbiased gene expression abundance estimation, we processed all downloaded RNA-seq samples starting from data quality checking step and quantified gene expression using the same protocol as has been done for analyzing control and *uxt* CKO retinas RNA-seq data.

Curated retinitis pigmentosa related gene list

To obtain retinitis pigmentosa-related gene list, we manually curated genes associated with retinitis pigmentosa based on [42,55,56] and merged them into a non-redundant gene list containing 71 retinitis pigmentosa-related genes in total.

Electroretinogram (ERG) and Fundus photography experiments

ERG responses were recorded in two groups, including 10 *uxt* CKO and 10 control P14 (postnatal) old littermates, and 10 *uxt* CKO and 10 control 1-month-old littermates. These mice were composed of male and female in equal. All animals were recorded under the same settings and conditions. Mice were dark-adapted overnight before ERG performed. Under weak red light, mice were anesthetized with intramuscular injection of ketamine (100 $\mu\text{g/g}$ body weight). Pupils were dilated by tropicamide phenylephrine eye drops, and corneas were kept moist with a drop of hypromellose. During ERG recording, mice were tested under dark adaptation first. Then, they were exposed to full-field scotopic flashes of 1.3 ms duration presented by the Espion E2 system and a Color Dome Ganzfeld stimulator (Diagnosys) with different intensities: 0.003, 0.01, 0.03, 0.1, 0.3, 1.0, 3.0, 10 cd.s/m^2 . Flash stimuli above 10 cd.s/m^2 were delivered by a Xenon lamp, and those below 10 cd.s/m^2 were delivered by a green (525 nm) LED. Mice were light-adapted with a saturating background (green, 20 cd.s/m^2) for 5 min. Five levels of stimuli were used for the photopic recordings (0.3, 1.0, 3.0, 10, 30 cd.s/m^2). The a-wave amplitude was measured from baseline to the first negative peak, and the b-wave amplitude was measured from a-wave trough to the next positive peak.

For fundus photography, the central retinas (radius of 3–4 disc diameters around the disc) of 10 *uxt* CKO and 10 control 1-month and 3-month-old littermates were examined by placing hypromellose and a coverslip on their corneas and using an operating microscope (Zeiss). We examined and photographed the eyes of mice using a mouse fundus camera (KOWA Genesis-Df) to examine the entire retina, including the peripheral retina up to the ora serrata, in all directions.

Statistical analysis

Except for statistical tests applied to analyze RNA-seq data and downstream functional enrichment and disease association, the rest of statistical analysis was performed using GraphPad Prism 6.0, Image pro plus 6.0 and Microsoft Excel computer programs. The results are expressed as

mean \pm SEM for experiments conducted at least in triplicates. Wilcoxon-Mann-Whitney test used to assess the difference between two groups, and a value of $p < 0.05$ is considered to be statistically significant.

Acknowledgments

We thank Dr. Xin Zhang (The First School of Clinical Medicine, Nanjing Medical University) for sharing 661W cell line. Dr. Chen Wang was supported by the National Natural Science Foundation of China (31730018, 81672029), National Key R&D Program of China (2016YFA0501800), the Jiangsu Innovative and Entrepreneurial Talents Program, the National New Drug Innovation Major Project of China (2017ZX09309027), the Open Project of State Key Laboratory of Natural Medicines (SKLNMZZCX201802), the “Double First-Class” Project of China Pharmaceutical University (CPU2018GF10), the Jiangsu Innovative and Entrepreneurial Talents Program. Dr. Haiyang Hu was supported by the National Natural Science Foundation of China (31601068), the Priority Academic Program Development of Jiangsu Higher Education Institutions (PAPD), the “Double First-Class” Project of China Pharmaceutical University (CPU2018GF10). Mr. Mingyu Pan was supported by the Postgraduate Research & Practice Innovation Program of Jiangsu Province (3322000026).

Disclosure statement

The authors declare no competing interests.

Funding

This work was supported by the National Natural Science Foundation of China [31601068]; National Natural Science Foundation of China [81672029]; National Natural Science Foundation of China [31730018]; “Double First-Class” Project of China Pharmaceutical University [CPU2018GF10]; Postgraduate Research & Practice Innovation Program of Jiangsu Province [3322000026]; Jiangsu Innovative and Entrepreneurial Talents Program, the National New Drug Innovation Major Project of China [2017ZX09309027]; National Key R&D Program of China [2016YFA0501800]; Open Project of State Key Laboratory of Natural Medicines [SKLNMZZCX201802]; “Double First-Class” Project of China Pharmaceutical University [CPU2018GF10]; Priority Academic Program Development of Jiangsu Higher Education Institutions [PAPD].

ORCID

Lele Zhang  <http://orcid.org/0000-0002-5595-3103>
Haiyang Hu  <http://orcid.org/0000-0002-5348-5641>

References

- [1] Brooks MJ, Chen HY, Kelley RA, et al. Improved retinal organoid differentiation by modulating signaling pathways revealed by comparative transcriptome analyses with development in vivo. *Stem Cell Reports*. 2019;13(5):891–905.
- [2] Chizzolini M, Galan A, Milan E, et al. Good epidemiologic practice in retinitis pigmentosa: from phenotyping to biobanking. *Curr Genomics*. 2011;12(4):260–266.
- [3] Hamel C. Retinitis pigmentosa. *Orphanet J Rare Dis*. 2006;1:40.
- [4] Trapani I, Puppo A, Auricchio A. Vector platforms for gene therapy of inherited retinopathies. *Prog Retin Eye Res*. 2014;43:108–128.
- [5] Kennan A, Aherne A, Humphries P. Light in retinitis pigmentosa. *Trends Genet*. 2005;21(2):103–110.
- [6] Moreno ML, Mérida S, Bosch-Morell F, et al. Autophagy dysfunction and oxidative stress, two related mechanisms implicated in retinitis pigmentosa. *Front Physiol*. 2018;9:1008.

- [7] Reme CE, Young RW. The effects of hibernation on cone visual cells in the ground squirrel. *Invest Ophthalmol Vis Sci.* 1977;16(9):815–840.
- [8] Kunchithapautham K, Rohrer B. Apoptosis and autophagy in photoreceptors exposed to oxidative stress. *Autophagy.* 2007;3(5):433–441.
- [9] Howell JJ, Dias MF, Joo K, et al. A growing role for mTOR in promoting anabolic metabolism. *Biochem Soc Trans.* 2013;41(4):906–912.
- [10] Punzo C, Kornacker K, Cepko CL. Stimulation of the insulin/mTOR pathway delays cone death in a mouse model of retinitis pigmentosa. *Nat Neurosci.* 2009;12(1):44–52.
- [11] Venkatesh A, Ma S, Punzo C. TSC but not PTEN loss in starving cones of retinitis pigmentosa mice leads to an autophagy defect and mTORC1 dissociation from the lysosome. *Cell Death Dis.* 2016;7(6):e2279.
- [12] Huang Y, Liu H, Ge R, et al. UXT-V1 facilitates the formation of MAVS antiviral signalosome on mitochondria. *J Immunol.* 2012;188(1):358–366.
- [13] Huang Y, Chen L, Zhou Y, et al. UXT-V1 protects cells against TNF-induced apoptosis through modulating complex II formation. *Mol Biol Cell.* 2011;22(8):1389–1397.
- [14] Sun S, Tang Y, Lou X, et al. UXT is a novel and essential cofactor in the NF-kappaB transcriptional enhanceosome. *J Cell Biol.* 2007;178(2):231–244.
- [15] Zhou Y, Ge R, Wang R, et al. UXT potentiates angiogenesis by attenuating Notch signaling. *Development.* 2015;142(4):774–786.
- [16] Schroer A, Schneider S, Ropers -H-H, et al. Cloning and characterization of UXT, a novel gene in human Xp11, which is widely and abundantly expressed in tumor tissue. *Genomics.* 1999;56(3):340–343.
- [17] Brzezinski JA, Reh TA. Photoreceptor cell fate specification in vertebrates. *Development.* 2015;142(19):3263–3273.
- [18] Chang GQ, Hao Y, Wong F. Apoptosis: final common pathway of photoreceptor death in rd, rds, and rhodopsin mutant mice. *Neuron.* 1993;11(4):595–605.
- [19] Gobe G, Crane D. Mitochondria, reactive oxygen species and cadmium toxicity in the kidney. *Toxicol Lett.* 2010;198(1):49–55.
- [20] Shi L, Chen J, Yang J, et al. MiR-21 protected human glioblastoma U87MG cells from chemotherapeutic drug temozolomide induced apoptosis by decreasing Bax/Bcl-2 ratio and caspase-3 activity. *Brain Res.* 2010;1352:255–264.
- [21] Boga TH, Wen RH, Moritz OL. Light induces ultrastructural changes in rod outer and inner segments, including autophagy, in a transgenic xenopus laevis P23H rhodopsin model of retinitis pigmentosa. *Invest Ophthalmol Vis Sci.* 2015;56(13):7947–7955.
- [22] Mizushima N, Yoshimori T, Levine B. Methods in mammalian autophagy research. *Cell.* 2010;140(3):313–326.
- [23] Kabeya Y, Mizushima N, Ueno T, et al. LC3, a mammalian homologue of yeast Apg8p, is localized in autophagosome membranes after processing. *Embo J.* 2000;19(21):5720–5728.
- [24] Haspel J, Shaik RS, Ifedigbo E, et al. Characterization of macroautophagic flux in vivo using a leupeptin-based assay. *Autophagy.* 2011;7(6):629–642.
- [25] Miller S, Oleksy A, Perisic O, et al. Finding a fitting shoe for Cinderella: searching for an autophagy inhibitor. *Autophagy.* 2010;6(6):805–807.
- [26] Settembre C, Di Malta C, Polito VA, et al. TFEB links autophagy to lysosomal biogenesis. *Science.* 2011;332(6036):1429–1433.
- [27] Settembre C, Zoncu R, Medina DL, et al. A lysosome-to-nucleus signalling mechanism senses and regulates the lysosome via mTOR and TFEB. *Embo J.* 2012;31(5):1095–1108.
- [28] Isotani S, Hara K, Tokunaga C, et al. Immunopurified mammalian target of rapamycin phosphorylates and activates p70 S6 Kinase α in Vitro. *J Biol Chem.* 1999;274(48):34493–34498.
- [29] Lin B, Xiong G, Yang W. Ribosomal protein S6 kinase 1 promotes the survival of photoreceptors in retinitis pigmentosa. *Cell Death Dis.* 2018;9(12):1141.
- [30] Thoreen CC, Kang SA, Chang JW, et al. An ATP-competitive mammalian target of rapamycin inhibitor reveals rapamycin-resistant functions of mTORC1. *J Biol Chem.* 2009;284(12):8023–8032.
- [31] Chen Y, Sawada O, Kohno H, et al. Autophagy protects the retina from light-induced degeneration. *J Biol Chem.* 2013;288(11):7506–7518.
- [32] Yao J, Jia L, Feathers K, et al. Autophagy-mediated catabolism of visual transduction proteins prevents retinal degeneration. *Autophagy.* 2016;12(12):2439–2450.
- [33] Zhou Z, Doggett TA, Sene A, et al. Autophagy supports survival and phototransduction protein levels in rod photoreceptors. *Cell Death Differ.* 2015;22(3):488–498.
- [34] Laplante M, Sabatini DM. mTOR signaling in growth control and disease. *Cell.* 2012;149(2):274–293.
- [35] Wullschlegel S, Loewith R, Hall MN. TOR signaling in growth and metabolism. *Cell.* 2006;124(3):471–484.
- [36] Ben-Sahra I, Manning BD. mTORC1 signaling and the metabolic control of cell growth. *Curr Opin Cell Biol.* 2017;45:72–82.
- [37] Lipton JO, Sahin M. The neurology of mTOR. *Neuron.* 2014;84(2):275–291.
- [38] Switon K, Kotulska K, Janusz-Kaminska A, et al. Molecular neurobiology of mTOR. *Neuroscience.* 2017;341:112–153.
- [39] Jomary C, Cullen J, Jones SE. Inactivation of the Akt survival pathway during photoreceptor apoptosis in the retinal degeneration mouse. *Invest Ophthalmol Vis Sci.* 2006;47(4):1620–1629.
- [40] Ivanovic I, Anderson RE, Le YZ, et al. Deletion of the p85alpha regulatory subunit of phosphoinositide 3-kinase in cone photoreceptor cells results in cone photoreceptor degeneration. *Invest Ophthalmol Vis Sci.* 2011;52(6):3775–3783.
- [41] Hartong DT, Berson EL, Dryja TP. Retinitis pigmentosa. *Lancet.* 2006;368(9549):1795–1809.
- [42] Dias MF, Joo K, Kemp JA, et al. Molecular genetics and emerging therapies for retinitis pigmentosa: basic research and clinical perspectives. *Prog Retin Eye Res.* 2018;63:107–131.
- [43] Talib M, van Schooneveld MJ, Thiadens AA, et al. Clinical and genetic characteristics of male patients with prgr-associated retinal dystrophies: a long-term follow-up study. *Retina.* 2019;39(6):1186–1199.
- [44] Chang B, Hawes NL, Hurd RE, et al. Retinal degeneration mutants in the mouse. *Vision Res.* 2002;42(4):517–525.
- [45] Bolger AM, Lohse M, Usadel B. Trimmomatic: a flexible trimmer for Illumina sequence data. *Bioinformatics.* 2014;30(15):2114–2120.
- [46] Kim D, Paggi JM, Park C, et al. Graph-based genome alignment and genotyping with HISAT2 and HISAT-genotype. *Nat Biotechnol.* 2019;37(8):907–915.
- [47] Zerbino DR, Achuthan P, Akanni W, et al. Ensembl 2018. *Nucleic Acids Res.* 2018;46(D1):D754–d761.
- [48] Liao Y, Smyth GK, Shi W. featureCounts: an efficient general purpose program for assigning sequence reads to genomic features. *Bioinformatics.* 2014;30(7):923–930.
- [49] Robinson MD, McCarthy DJ, Smyth GK. edgeR: a bioconductor package for differential expression analysis of digital gene expression data. *Bioinformatics.* 2010;26(1):139–140.
- [50] Huang DW, Sherman BT, Tan Q, et al. DAVID bioinformatics resources: expanded annotation database and novel algorithms to better extract biology from large gene lists. *Nucleic Acids Res.* 2007;35(suppl_2):W169–75.
- [51] Becker KG, Barnes KC, Bright TJ, et al. The genetic association database. *Nat Genet.* 2004;36(5):431–432.
- [52] Herrero J, Muffato M, Beal K, et al. Ensembl comparative genomics resources. *Database (Oxford).* 2016;2016:baw053.
- [53] Shen Y, Yue F, McCleary DF, et al. A map of the cis-regulatory sequences in the mouse genome. *Nature.* 2012;488(7409):116–120.
- [54] Hoshino A, Ratnapriya R, Brooks MJ, et al. Molecular anatomy of the developing human retina. *Dev Cell.* 2017;43(6):763–779.e4.
- [55] Daiger SP, Sullivan LS, Bowne SJ. Genes and mutations causing retinitis pigmentosa. *Clin Genet.* 2013;84(2):132–141.
- [56] Daiger SP, Bowne SJ, Sullivan LS. Genes and mutations causing autosomal dominant retinitis pigmentosa. *Cold Spring Harb Perspect Med.* 2014;5(10):a017129.